

On the Nanoscale Electromechanical Wireless Communication in the VHF Band

Janne J. Lehtomäki, *Member, IEEE*, A. Ozan Bicen, *Student Member, IEEE*, and Ian F. Akyildiz, *Fellow, IEEE*

Abstract—Electromagnetic communication at the nanoscale has, to date, been studied in either the very high frequency (VHF) (30–300 MHz) or in the TeraHertz band (0.1–10 THz). The main focus of this paper is on electromagnetic communication in the VHF band and determining the bit error rate (BER) performance of nanoscale receivers utilizing a carbon nanotube (CNT). To determine BER performance, statistical characterization of an average-level detector output is obtained for two different receiver configurations: nanotube receiver, and tunneling nanotube receiver. For the nanotube receiver, the linear component not considered in the previous studies is included and shown to significantly affect the variance of the detector output and, also, exact analysis is performed with some significant differences to previous approximations. The tunneling nanotube receiver, for which no statistical characterization has been done to date, is analyzed. Extensive simulation studies are presented to confirm the accuracy of the theoretical results provided for the distribution of the average-level detector output. The feasible communication distances are investigated based on the BER performance by using realistic system parameters. The results reveal the potential usage of the VHF band in nanonetworks and highlight the importance of maximizing the charge at the CNT tip.

Index Terms—Carbon nanotubes, field emission, tunneling effect, nanonetworks, nanomachines, VHF band, wireless communication.

I. INTRODUCTION

NANOMACHINES consist of nanoscale components such as sensing, power, processing, data storage, and communication units. Nanomachines can form a nanonetwork to perform cooperative operation for many applications in nanoscale environments [1]. Envisioned applications of these nanonetworks include air pollution control, monitoring the condition of crops in farming, health monitoring, controlled drug delivery, smart garbage processing to help biodegradation, interconnected offices, and even bio-hybrid implants [2]–[4].

Manuscript received June 13, 2014; revised September 27, 2014 and November 27, 2014; accepted November 30, 2014. Date of publication December 8, 2014; date of current version January 14, 2015. This work was supported by the U.S. National Science Foundation (NSF) under Grant No. CCF-1349828. The associate editor coordinating the review of this paper and approving it for publication was E. Perrins.

J. J. Lehtomäki was with Broadband Wireless Networking Lab, Georgia Institute of Technology, Atlanta, GA, 30332, USA. He is now with the Centre for Wireless Communications (CWC), Department of Communications Engineering, University of Oulu, Oulu, Finland (e-mail: jannel@ee.oulu.fi).

A. O. Bicen and I. F. Akyildiz are with the Broadband Wireless Networking Lab, School of Electrical and Computer Engineering, Georgia Institute of Technology, Atlanta, GA 30332 USA (e-mail: bozan@ece.gatech.edu; ian@ece.gatech.edu).

Color versions of one or more of the figures in this paper are available online at <http://ieeexplore.ieee.org>.

Digital Object Identifier 10.1109/TCOMM.2014.2379254

It is beneficial to conduct communication theoretic research in parallel to hardware-oriented research aiming to develop complete nanomachines [1]. An “ant-sized” (3.7 mm × 1.2 mm chip) power-harvesting radio operating at 24 GHz and 60 GHz has been recently demonstrated [5]. This demonstrates the trend towards smaller and smaller radios operating at higher frequencies than before, and radios with energy harvesting. Inevitably, this trend will lead to integrated nanodevices. Recently, nanowire computer with 180 transistors has been experimentally demonstrated [6]. As mentioned therein, this suggests that in the near-future general purpose nanoprocessors can be realized.

Recent studies show that a single mechanically oscillating carbon nanotube (CNT) constitutes the four fundamental components of a receiver, i.e., antenna, filter, amplifier, and demodulator [7], [8]. The frequency range of CNT-based receivers utilizing mechanical oscillations is within the very high frequency (VHF) band ranging from 30–300 MHz. The VHF band has a much reduced path loss compared to the THz band, which was determined to be the frequency band to use for nanoscale networks in [9]. We believe that CNT-based reception using mechanical oscillations in the VHF band is a promising frequency alternative for nanonetworks. Furthermore, a CNT-based receiver contains its own antenna [7], so that it can benefit from reduced path loss in the VHF band without a large antenna. Despite its extremely small size, the nanotube has the potential to collect radiation over a relatively large area [8]. It has also been shown that a CNT or a graphene-based mechanical oscillator can be used to develop the transmitter circuitry [10], [11]. In this paper we focus on the receivers that use a CNT.

The first demonstration of a CNT-based receiver used the field emission effect with a CNT of approximately 500 nm long [7], [8]. Moreover, an experimental demonstration showed that audio signals could be received over a wireless channel [7], [8]. Recent [12] utilizes a similar receiver as [7], [8] but with nanopillars instead CNTs. A fabrication method for nanopillars enabling accurate positioning is also presented. Experimental tests verify that audio signals can be received with a nanopillar array. The same theoretic principles apply to nanopillars as to CNTs even through nanopillars are significantly larger than CNTs. A proof-of-concept is provided by simulations of a CNT-based receiver using the tunneling effect in [13]. In [14], a nanotube suspended between two electrodes was used for demodulation, operation as antenna is not included and an external source connected to the electrodes is assumed. In the remainder of this paper we use the **nanotube receiver** from [7], [8] and the **tunneling nanotube receiver** from [13]. Both of these receivers are based on mechanical oscillations of a CNT

attached to an electrode, caused by the electromagnetic (EM) communication signal and the associated electric field. The use of mechanical oscillations enables these nanoscale receivers to work at very low frequencies. These mechanical oscillations can be detected by using the field emission effect (in nanotube receivers) or quantum tunneling effect (in tunneling nanotube receivers) as described in [7], [8], [13]. In both of these receivers, electrons move from the CNT tip to a nearby counter electrode leading to output current enabling reception. The differences between nanotube and tunneling nanotube receivers are in the applied voltages (between the electrodes) and the distances between the CNT tip and the counter-electrode. The nanotube receiver requires the use of voltages ranging from 30–300 V [7], [15], [16] while the tunneling nanotube receiver requires 10 V or less [13]. The nanotube receiver has relaxed requirements in terms of distances while the tunneling nanotube receiver requires distance of a few nm [8]. The difference in terms of the communication theoretic aspect, (this is the focus of our paper) is that the equations governing the relationship between the input and output are different for both cases.

The communication theory aspect of the nanotube receiver only is investigated in [17], [18]. The mean and variance of the decision variable are determined for the nanotube receiver for digital communication by using On/Off keying with a tone signal to calculate the bit error rates (BER). However, only the second order component is considered in the relationship between the input and output in the nanotube receiver and the linear component was not considered at all. Reference [19] presents the first communication theoretical analysis of nanoscale optical communication in the 300–700 THz band. Therein, CNTs are used as photodiodes and performance is evaluated for multiple noise types which are typical in optical receivers. For digital radio frequency (RF) communication, there is so far no analysis incorporating the linear component in the received signal which affects the performance significantly, as will be shown in our analysis. Furthermore, the communication theoretic analysis of the tunneling nanotube receiver is also missing in the literature so far.

In this paper, we consider the performance of the nanotube receivers and the tunneling nanotube receivers for digital communication by using the existing physical models. To reveal the actual digital communication performance, we find exact statistics of the decision variable for both nanotube receivers and tunneling nanotube receivers by first deriving an exact correlation function for the colored noise component affecting the decision variable used for determining the received bit. Our analysis of nanotube receiver includes the second order, linear, and constant components in the received signal to provide more accurate characterization of digital communication performance. The utilized parameters for nanotube receiver are based on real measurements [16]. Our main contributions in this paper are:

1) **Statistical characterization of the decision variable:**

For nanotube receiver we show that the linear component, which has not been considered in the previous studies, significantly affects the variance and must be included in the analysis. In addition to including the linear component, we also perform exact analysis for the mean and

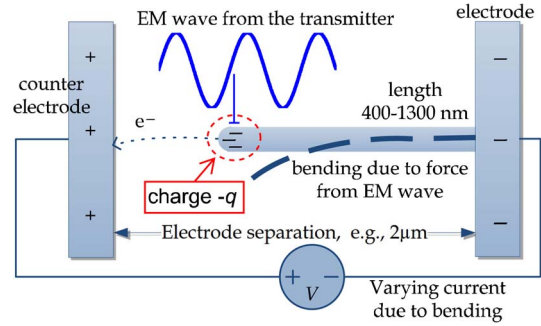


Fig. 1. Nanotube radio receiver.

variance. We determine that the difference to the previous approximation studies [17], [18] is significant for the variance in the noise-only (Off) case. We also find the mean and variance for tunneling nanotube receiver for which statistical characterization has not been considered to date.

- 2) **Digital communication performance:** We evaluate the communication range with On/Off keying for nanotube and tunneling nanotube receivers. Previously, these communication ranges have not been determined at all. Our results show that, although communication distances are not sufficient for terrestrial radio communication with long link distances, they are suitable for use in nanonetworks. The developed expressions are validated by simulations based on highly oversampled RF signals.

The remainder of this paper is organized in the following manner. In Section II, we explain the utilized signal model for nanotube and tunneling nanotube receivers. We discuss how an electric field at a receiver will lead to output current. Then in Section III we explain how the receiver's output current can be used for digital communication with average-level detection and On-Off keying. To evaluate the bit error rate performance, we derive expressions for the mean and variance of the average level detector output for both noise and signal with noise cases for the nanotube receiver in Section IV and for the tunneling nanotube receiver in Section V. The numerical and simulation results are presented in Section VI. Effects of the CNT's size parameters are discussed in Section VII. Finally, we conclude the paper in Section VIII.

II. ELECTROMECHANICAL SIGNAL CONVERSION AT NANOTUBE RECEIVER

The nanotube receiver circuitry developed in [7] is illustrated in Fig. 1. The CNT is attached to an electrode, and there is a counter-electrode close by. A DC voltage V is applied between the electrodes. This voltage yields the accumulation of negatively charged electrons at the tip of the nanotube as shown in Fig. 1. Therefore, the electric field associated with the incoming EM transmission leads to the displacement of the tip of the nanotube, i.e., *mechanical oscillation*, due to forces on the charge $-q$, where q is the absolute total value of the charge from the negatively charged electrons. The receiver is enclosed in a few micrometers long vacuum container to increase the induced current, reduce noise effects, and protect the CNT radio.

Note that the vacuum container can also cause a limitation for downgrading the CNT radio size, reduction of which requires special investigation and beyond the scope of our work.

In the following subsections, we present the model for mechanical oscillations, and then, we formulate the induced electrical current at the nanotube receiver and tunneling nanotube receiver.

A. Induced Mechanical Oscillations by Electric Field and Noise

The mechanical oscillation of the tip of the nanotube is characterized by the time-variant vertical displacement $y(t)$ (in the vertical axis of Fig. 1). The mechanical oscillation can be caused by received electric field from a transmitter and thermomechanical noise. First, we show the mechanical transfer function for relationship between the electric field and $y(t)$. Then we show the noise component in $y(t)$.

1) *Mechanical Transfer Function*: The frequency response of the vertical displacement for an incoming electric field with frequency f can be found as [7]

$$|H_{\text{mech}}(f)| = \frac{q/m_{\text{eff}}}{\sqrt{(4\pi^2 f^2 - \omega_0^2)^2 + \left(\frac{2\pi f \omega_0}{Q}\right)^2}}, \quad (1)$$

where m_{eff} is the effective mass of the CNT, Q is the quality factor of the CNT (typically ~ 400 – 800), and ω_0 is the resonance frequency of the CNT.

The response is strongest when $\omega = 2\pi f$ is close to the resonance frequency ω_0 . The resonance frequency of the first mode can be derived using the Euler-Bernoulli beam theory as $\omega_0 = 2\pi c_e/L^2$, where L is the length of the CNT and c_e is a constant dependent on the physical dimensions of the CNT and Young's modulus, the calculation of which is given in [7].

The time constant for the oscillation, i.e., the required duration to reach 63% of its steady-state amplitude, is $\tau = 2Q/\omega_0$ [20]. The higher quality factor Q yields improved frequency resolution and higher steady-state gain. However, the higher quality factor also leads to an increased transient duration, limiting the available communication rate [20].

2) *Mechanical Noise*: The CNT vibrates due to thermal energy even when no electric field is present. The vertical displacement due to thermal energy is represented by $y_{\text{noise}}(t)$. Based on the equipartition theorem [20]

$$E(y_{\text{noise}}(t)^2) = \frac{k_B T_K}{m_{\text{eff}} \omega_0^2}, \quad (2)$$

where $E(\cdot)$ denotes expectation, k_B is the Boltzmann constant and T_K is the temperature in Kelvin. The corresponding one-sided power spectral density (PSD) is given by [20], [21]

$$N_{\text{th}}(f) = \frac{4k_B T_K \omega_0}{Q m_{\text{eff}} \left[(4\pi^2 f^2 - \omega_0^2)^2 + (2\pi f \omega_0 / Q)^2 \right]}. \quad (3)$$

This PSD follows due to the fluctuation-dissipation theorem [22]. It should be noted that in practical CNTs other noise sources such as adsorption-desorption noise, and tension noise can be dominant [8]. Following [8], we only consider thermomechanical noise, which is shown to ultimately limit the

performance. We also point out that in atomic force microscopy (AFM) also oscillations based on the thermal vibrations are dominant [20]. The noise effect for (3) can be taken as a white Gaussian stationary noise process with one-sided PSD [17], [20], [22] as

$$N_a = \frac{4m_{\text{eff}} k_B T_K \omega_0}{Q q^2} \quad (4)$$

which drives the CNT with frequency response given by (1). Background radio noise in the VHF band could also be modeled by incrementing N_a by the PSD of the ambient noise.

B. Electrical Current Conversion: Vertical Displacement $y(t) \rightarrow$ Output Current

We approximate to our analysis the nanotube receiver [7], [16] and the tunneling nanotube receiver [13] with quadratic and exponential current conversion functions, respectively.

1) *Quadratic Current Conversion Function*: Based on Fowler-Nordheim law the field electron emission output current can be modeled with [15], [16]

$$I(y(t)) = A_1 (\beta(y(t)) V)^2 \exp\left(-\frac{B_1}{\beta(y(t)) V}\right), \quad (5)$$

where A_1 and B_1 are constants given in [16] and $\beta(y(t))$ is the local field enhancement factor which can be approximated with [16]

$$\beta(y(t)) = \beta_0 + \beta_1 y(t) + \beta_2 y(t)^2, \quad (6)$$

where β_0 , β_1 , and β_2 based on electrostatic calculations and real experiments are given in [16].

By using (6) in (5) and utilizing Taylor series approximation (as in [16]) of $I(y(t))$ in terms of $y(t)$ we get quadratic function approximation of $I(y(t))$ as

$$g_1(y(t)) = I_0 \alpha_2 y(t)^2 + I_0 \alpha_1 y(t) + I_0, \quad (7)$$

where $g_1(y(t))$ represents an approximation to $I(y(t))$ and

$$\alpha_2 = \left(\frac{2\beta_2}{\beta_0} + \frac{\beta_1^2}{\beta_0^2} + \frac{B_1^2 \beta_1^2}{2V^2 \beta_0^4} + \frac{B_1 \beta_2}{V \beta_0^2} + \frac{B_1 \beta_1^2}{V \beta_0^3} \right), \quad (8)$$

$$\alpha_1 = \beta_1 \left(\frac{B_1 + 2V \beta_0}{V \beta_0^2} \right), \quad (9)$$

and the zero displacement ($y(t) = 0$) current is

$$I_0 = A_1 (\beta_0 V)^2 \exp\left(-\frac{B_1}{\beta_0 V}\right). \quad (10)$$

The accuracy of this approximation is shown in Fig. 2 using parameters corresponding to [16, Table I]. These parameters correspond to a slightly tilted CNT resulting the maximum current being obtained with a negative transverse displacement y . In the figure, we also show results for $I_0 \alpha_2 y^2 + I_0$ since later it will be shown that it is enough for analyzing the mean of the decision variable. However, for variance, the linear component needs to be included.

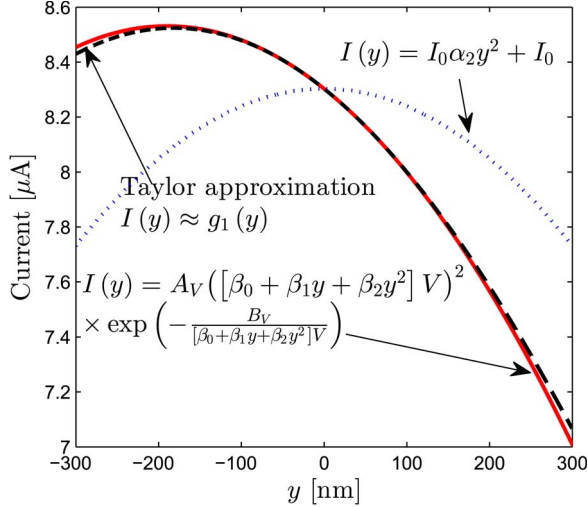


Fig. 2. Taylor approximation of nanotube receiver output current as a function of the CNT tip transverse displacement y .

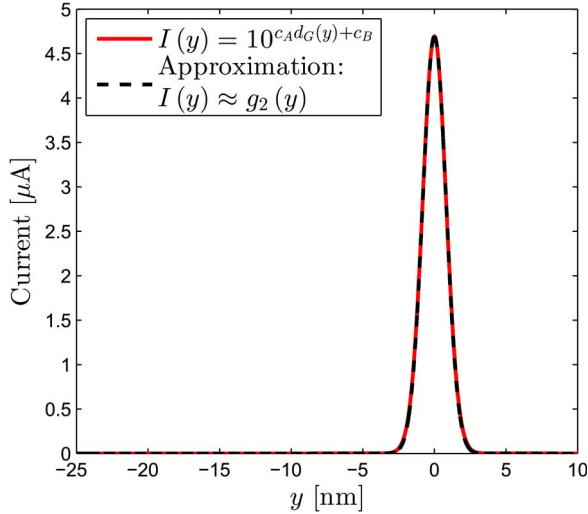


Fig. 3. Approximation of tunneling nanotube receiver output current, $c_A = -3.2681 \times 10^9$, $c_B = 11.0121$, $d_{Gap,0} = 5$ nm.

2) *Exponential Current Conversion Function*: The exponential relationship can be used to model output current as a function of gap distance [23], i.e.,

$$I(y(t)) = 10^{c_A d_{Gap}(y(t)) + c_B}, \quad (11)$$

where c_A and c_B are parameters and $d_{Gap}(y(t)) = \sqrt{d_{Gap,0}^2 + y(t)^2}$ is the gap between the CNT tip and a sharp counter-electrode [13] with $d_{Gap,0}$ denoting the tunneling gap in the rest position. We approximate $I(y(t))$ given by (11) with

$$g_2(y(t)) = c_1 \exp(-c_2 y(t)^2), \quad (12)$$

where $c_1 = 10^{c_B + c_A d_{Gap,0}}$ and $c_2 = -\ln(10)c_A / (2d_{Gap,0})$. Its accuracy is verified in Fig. 3.

The tunneling nanotube receiver in [13] corresponds to $c_A = -3.2681 \times 10^9$, $c_B = 11.0121$, $d_{Gap,0} = 5$ nm. It can be seen in Fig. 3 that the tunneling nanotube receiver is sensitive for small vertical displacement of the CNT tip.

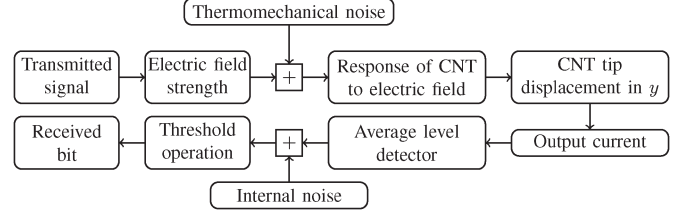


Fig. 4. Digital communication model based on On-Off keying.

III. COMMUNICATION MODEL

In Fig. 4, we show the communication model which we will consider in the remainder of our paper. We see two main scenarios for using nanotube and tunneling nanotube receivers in nanonetworks: 1) Broadcast communication for downlink from a portable macro-scale transmitter close enough to the nanonetwork to be controlled to enable sufficient electric field strength at the nanoscale receivers, i.e., within a few meters; 2) for nanomachine to nanomachine links with very short communication distances, i.e., in the order of a few millimeters [24].

A. Modulation Scheme and Transmitted Signal

Amplitude modulated (AM) audio signal has been used in [7], [8]

$$s_{AM}(t) = A [1 + h \cos(2\pi f_L t)] \cos(2\pi f_c t + \theta), \quad (13)$$

where A is the amplitude, $h < 1$ is the modulation index, f_L is the frequency of the modulating signal, f_c is the carrier frequency, and θ is random carrier phase. For digital communication where the purpose is to transmit bits we utilize a sinusoidal tone with On-Off keying similar as in [17], i.e., the transmitted signal in the On state corresponding to bit 1 is

$$s_{CW}(t) = A \cos(2\pi f_c t + \theta) \quad (14)$$

and in the Off state (bit 0) nothing is transmitted. As an example of the demodulation, let us consider how square-law operation will affect the above signals. For noiseless AM signal,

$$\begin{aligned} \frac{s_{AM}(t)^2}{A^2} &= \left(\frac{1}{2} + \frac{h^2}{4} \right) + h \cos(2\pi f_L t) + \frac{h^2}{4} \cos(4\pi f_L t) \\ &+ \cos(4\pi f_c t + 2\theta) \left[\frac{1}{2} + \frac{h^2}{4} + h \cos(2\pi f_L t) + \frac{h^2}{4} \cos(4\pi f_L t) \right] \end{aligned} \quad (15)$$

which contains a DC term, the desired term with the correct modulation message frequency, a double frequency term, and a radio carrier frequency term.

Although the AM is intended for audio signals, it can be applied for digital communication by using two (or more) modulation frequencies ($f_{L,1}$ and $f_{L,2}$) one of which represents bit 0 and the another one represents bit 1. This is frequency shift keying (FSK) modulating an RF carrier using AM, similar to audio FSK (AFSK). In noncoherent demodulation, we can use two bandpass filters followed by envelope detectors and find the larger output.

In this work, we do not consider AFSK due to the required complexity for demodulation. For our preferred signal, the sinusoidal signal, the square-law operation leads to

$$s_{CW}(t)^2 = \frac{A^2}{2} + \frac{A^2}{2} \cos(4\pi f_c t + 2\theta), \quad (16)$$

which contains a DC term and a radio frequency term.

B. Received Signal

1) *Electric Field Strength at the Receiver:* We assume the standard free space channel model, and the utilization of other channel effects such as shadowing or scattering on the path is left for future work. By using the impedance of the free space (120π), we get the electric field strength

$$E_{\text{rad}} = \sqrt{P_T 10^{\frac{G}{10}} \frac{\sqrt{60}}{d}}, \quad (17)$$

where P_T is power used for transmission in [W], G is the gain of the transmitting antenna in [dBi] and d is the distance between transmitter and receiver in [m]. This equation is based on the far field theory so for very short communication distances the field strength is much higher.

2) *CNT Tip Displacement $y(t)$ and Output Current:* Let us use *recv* to denote the case with both signal and noise (On) and *noise* to denote the noise-only case (Off). Now the CNT tip displacement $y(t)$ can be represented as

$$y(t) = \begin{cases} y_{\text{recv}}(t) & \text{bit} = 1 \\ y_{\text{noise}}(t) & \text{bit} = 0, \end{cases} \quad (18)$$

where $y_{\text{noise}}(t)$ is the colored Gaussian noise resulting from feeding the white Gaussian noise with one-sided PSD N_a given in (4) through the filter H_{mech} corresponding to (1). For the signal with noise case, $y_{\text{recv}}(t) = y_s(t) + y_{\text{noise}}(t)$ and $y_s(t)$ is the received signal component (electric field) filtered with H_{mech} . We map the CNT tip displacement to output current for the nanotube and tunneling nanotube receivers by using functions (7) and (12), respectively, leading to time varying output current $I(y(t))$. The current conversion functions are operating on the noisy CNT tip transverse displacement $y(t)$. The fundamental performance limits come from the signal-to-noise-ratio between the signal component $y_s(t)$ and the noise component $y_{\text{noise}}(t)$.

The nanotube receiver output current (7) always includes the component I_0 . DC cancellation to remove I_0 would remove also a big part of the signal component coming from the square-law term $I_0 \alpha_2 y(t)^2$, where $y(t)$ is defined in (18) and multiplication of square-law term with $I_0 \alpha_2$ comes from (7). The varying DC level makes blocking only I_0 challenging. To keep the receiver simple and for protecting important signal components we do not assume any DC blocks.

C. Average-Level Detector and Threshold Setting

Following [13], [17], we use an average-level detector to detect the presence of a signal. Therefore, the utilized decision

statistic for both nanotube and tunneling nanotube receivers is

$$\xi = \frac{1}{T} \int_{t=0}^T I(y(t)) dt, \quad (19)$$

where T is the bit interval. Here the time index $t = 0$ denotes the start of the considered bit interval. The synchronization errors would reduce the signal component in the detector output and/or cause intersymbol interference (ISI).

Basically, the presence of a signal will *reduce* the output current level and this can be used to detect the presence of a signal with a threshold λ to separate bit 0 and bit 1. The reduction of the output current due non-zero y can be observed in Fig. 3. This reduction also occurs in the case of nanotube receiver (Fig. 2) since (as shown later by the analysis) for the nanotube receiver the coefficient α_1 in (7) can be ignored when finding the mean of the detector output. However, the linear component scaled by α_1 cannot be ignored when finding the variances.

To model the internal noise (such as thermal noise) of the receiver, we add an additive zero-mean Gaussian random variable v with variance σ_{int}^2 to the detector output, i.e.,

$$\eta = \xi + v, \quad (20)$$

where η is the detector output with internal noise and ξ is the detector output without internal noise (but with thermomechanical noise and any possible signals). Thus

$$E(\eta_{\text{noise}}) = E(\xi_{\text{noise}}) \quad (21)$$

$$E(\eta_{\text{recv}}) = E(\xi_{\text{recv}}) \quad (22)$$

$$\text{Var}(\eta_{\text{noise}}) = \text{Var}(\xi_{\text{noise}}) + \sigma_{\text{int}}^2 \quad (23)$$

$$\text{Var}(\eta_{\text{recv}}) = \text{Var}(\xi_{\text{recv}}) + \sigma_{\text{int}}^2, \quad (24)$$

where $\text{Var}(\cdot)$ denotes the variance and subscript *noise* refers to the noise-only case and *recv* refers to the signal with noise case. Assuming equiprobable bits we find the BER with

$$\text{BER}(\lambda) = \frac{1}{2} \text{Prob}(\eta_{\text{noise}} \leq \lambda) + \frac{1}{2} \text{Prob}(\eta_{\text{recv}} > \lambda). \quad (25)$$

By invoking the Gaussian approximation

$$\text{BER}(\lambda) = \frac{1}{2} \left(1 - Q_{\text{func}} \left(\frac{\lambda - E(\eta_{\text{noise}})}{\sqrt{\text{Var}(\eta_{\text{noise}})}} \right) \right) + \frac{1}{2} Q_{\text{func}} \left(\frac{\lambda - E(\eta_{\text{recv}})}{\sqrt{\text{Var}(\eta_{\text{recv}})}} \right), \quad (26)$$

where $Q_{\text{func}}(\cdot)$ denotes the tail probability of standard normal distribution. The two critical points for this are given in the by (68) in Appendix B. The critical point leading to smaller BER gives the optimal threshold. We point out that in principle another critical point can also be used [17]. For example when $\text{Var}(\eta_{\text{recv}}) > \text{Var}(\eta_{\text{noise}})$ we could decide bit 1 if η is less than the first threshold or larger than the second threshold. Since this leads to only small gains for the studied receivers, we use only one threshold and assume that the optimal threshold λ^* from (68) is used.

IV. MEAN AND VARIANCE WITH THE QUADRATIC CURRENT CONVERSION FUNCTION

In this Section, we derive the mean and variance of the average-level detector output for both noise and signal with noise cases for the quadratic current conversion function (7) to obtain theoretical results for the bit error rate for the On-Off keying with the nanotube receiver [7], [8].

A. Noise Analysis

By utilizing the resonator's noise-equivalent bandwidth

$$W_{NE} = \pi f_0 / 2Q, \quad (27)$$

we get

$$\begin{aligned} E(\xi_{\text{noise}}) &= \frac{I_0 \alpha_2}{T} \int_{t=0}^T E[y_{\text{noise}}^2(t)] dt + I_0 \\ &= I_0 \alpha_2 N_a \cdot W_{NE} \cdot |H_{\text{mech}}(f_0)|^2 + I_0. \end{aligned}$$

Variance for noise (thermomechanical) only case is obtained with (see [25])

$$\text{Var}(\xi_{\text{noise}}) = \frac{1}{T} \int_{\tau=-T}^T (1 - |\tau|/T) C_{g_1(y_{\text{noise}})}(\tau) d\tau, \quad (28)$$

where $C_{g_1(y_{\text{noise}})}(\cdot)$ denotes autocovariance of the process $g_1(y_{\text{noise}}(t))$ and $g_1(\cdot)$ is given in (7). Let us denote $x = y_{\text{noise}}(t_1)$ and $y = y_{\text{noise}}(t_2)$ and $\tau = t_2 - t_1$. x and y follow the bivariate normal distribution, i.e.,

$$[x, y] \sim \mathcal{N}\left([0, 0], \begin{bmatrix} C_{y_{\text{noise}}}(0) & C_{y_{\text{noise}}}(\tau) \\ C_{y_{\text{noise}}}(\tau) & C_{y_{\text{noise}}}(0) \end{bmatrix}\right), \quad (29)$$

where the autocovariance $C_{y_{\text{noise}}}(\cdot)$ of the noise process $y_{\text{noise}}(t)$ is derived in the Appendix A. It is straightforward to show that $E[y_{\text{noise}}^2(t)] = N_a \cdot W_{NE} \cdot |H_{\text{mech}}(f_0)|^2 = C_{y_{\text{noise}}}(0)$ and thus

$$E(\xi_{\text{noise}}) = I_0 \alpha_2 C_{y_{\text{noise}}}(0) + I_0 \quad (30)$$

By definition $C_{g_1(y_{\text{noise}})}(\cdot)$ is

$$\begin{aligned} C_{g_1(y_{\text{noise}})}(\tau) &= E[(g_1(x) - E(\xi_{\text{noise}}))(g_1(y) - E(\xi_{\text{noise}}))] \\ &= E[g_1(x)g_1(y)] - E(\xi_{\text{noise}})^2 \\ &= I_0^2 E[(\alpha_2 x^2 + \alpha_1 x + 1)(\alpha_2 y^2 + \alpha_1 y + 1)] - E(\xi_{\text{noise}})^2. \end{aligned} \quad (31)$$

By using the Isserlis' theorem [26] for moments of multivariate normal distribution we get

$$\begin{aligned} C_{g_1(y_{\text{noise}})}(\tau) &= I_0^2 (\alpha_1^2 E(xy) + \alpha_1 \alpha_2 E(x^2 y) + \alpha_1 \alpha_2 E(x y^2) \\ &\quad + \alpha_1 E(x) + \alpha_1 E(y) \\ &\quad + \alpha_2^2 E(x^2 y^2) + \alpha_2 E(x^2) + \alpha_2 E(y^2) + 1) \\ &\quad - I_0^2 [\alpha_2 C_{y_{\text{noise}}}(0) + 1]^2 \end{aligned}$$

$$\begin{aligned} &= I_0^2 \alpha_1^2 C_{y_{\text{noise}}}(\tau) + I_0^2 \alpha_2^2 [C_{y_{\text{noise}}}(0)^2 + 2C_{y_{\text{noise}}}(\tau)^2] \\ &\quad + I_0^2 2\alpha_2 C_{y_{\text{noise}}}(0) + I_0^2 \\ &\quad - I_0^2 \alpha_2^2 C_{y_{\text{noise}}}(0)^2 - 2I_0^2 \alpha_2 C_{y_{\text{noise}}}(0) - I_0^2 \\ &= I_0^2 \alpha_1^2 C_{y_{\text{noise}}}(\tau) + 2I_0^2 \alpha_2^2 C_{y_{\text{noise}}}(\tau)^2. \end{aligned} \quad (32)$$

The variance can now be obtained by substituting above result to (28). Let us separate the resulting integral into parts as

$$\begin{aligned} \text{Var}(\xi_{\text{noise}}) &= \frac{1}{T} \int_{\tau=-T}^T (1 - |\tau|/T) I_0^2 \alpha_1^2 C_{y_{\text{noise}}}(\tau) d\tau \\ &\quad + \frac{1}{T} \int_{\tau=-T}^T (1 - |\tau|/T) 2I_0^2 \alpha_2^2 C_{y_{\text{noise}}}(\tau)^2 d\tau \\ &= \text{Var}(\xi_1) + \text{Var}(\xi_2). \end{aligned} \quad (33)$$

By substituting (61) (from Appendix A) and performing the integration, we get the exact result

$$\begin{aligned} \text{Var}(\xi_1) &= -\frac{\overline{\omega}}{T} (I_0 \alpha_1)^2 \\ &\quad \times \left(\frac{2}{u^2(u-v)} - \frac{2}{v^2(u-v)} - \frac{2}{T u^3(u-v)} \right. \\ &\quad \left. + \frac{2}{T v^3(u-v)} + \frac{2e^{-Tu}}{T u^3(u-v)} - \frac{2e^{-Tv}}{T v^3(u-v)} \right) \end{aligned} \quad (34)$$

where $\overline{\omega}$, u , and v are defined in the Appendix A. By using the definitions of u and v we get an expression involving only real-valued variables. To get an approximation, we note that in practical systems the quality factor $Q \gg 1$ and the bit interval should be much longer than transient duration, so $T\omega_0 \gg 2Q$. Therefore, the real component in $-Tu$ and $-Tv$ has a large negative value so we can ignore the exponential components involving these. We get

$$\begin{aligned} \text{Var}(\xi_1) &\approx \frac{\overline{\omega}}{T} I_0^2 \alpha_1^2 \left(\frac{2(Q^2 + QT\omega_0 - 1)}{Q^2 T \omega_0^4} \right) \\ &\approx \frac{2\overline{\omega} I_0^2 \alpha_1^2}{T} \left(\frac{Q + T\omega_0}{QT\omega_0^4} \right) \\ &\approx \frac{2\overline{\omega} I_0^2 \alpha_1^2}{T} \left(\frac{1}{Q\omega_0^3} \right) = \frac{I_0^2 \alpha_1^2}{T} \frac{N_a}{2Q^2} |H_{\text{mech}}(f_0)|^2 \end{aligned} \quad (35)$$

Similarly, by substituting (61) (from Appendix A) into (33) and integrating the second term, we get the exact result for $\text{Var}(\xi_2)$ presented in (69) in Appendix C, for which we obtain an approximation with similar assumptions as we used for $\text{Var}(\xi_1)$

$$\begin{aligned} \text{Var}(\xi_2) &\approx \frac{\overline{\omega}^2 I_0^2 \alpha_2^2}{T^2} \left(\frac{-2Q^4 + 2Q^3 T \omega_0 + 2QT\omega_0 - 1}{Q^2 \omega_0^6} \right) \\ &\approx \frac{\overline{\omega}^2 I_0^2 \alpha_2^2}{T^2} \left(\frac{-2Q^4 + 2Q^3 T \omega_0 + 2QT\omega_0}{Q^2 \omega_0^6} \right) \\ &\approx \frac{\overline{\omega}^2 I_0^2 \alpha_2^2}{T} \frac{2Q}{\omega_0^5} \\ &= \frac{I_0^2 \alpha_2^2}{T} \frac{W_{NE}}{2} \left(N_a |H_{\text{mech}}(f_0)|^2 \right)^2 \end{aligned} \quad (36)$$

This result can also be obtained by starting from the unconverted RC-noise model represented by (67) in Appendix A by following the similar assumptions. This result derived by using the exact noise process correlation function differs significantly from the one given in [17, eq. (15)] obtained by assuming that the autocovariance of squared noise process is a Dirac delta function. We can, however, modify their approach to include a width component W to get the same result. Let us study the square-law component of the noise and assume that in (28) the term $(1 - |\tau|/T)$ is decaying slowly as compared to the autocovariance of the squared noise process. Using approximation (67) in Appendix,

$$C_{y_{\text{noise}}^2}(\tau) = 2C_{y_{\text{noise}}}(\tau)^2 \approx \frac{2\omega_0^2}{\omega_0^4} e^{-\frac{\omega_0|\tau|}{Q}} \cos^2(\omega_0|\tau|) \quad (37)$$

By integrating this to get the area it contains and by setting the height of equivalent rectangle to be $C_{y_{\text{noise}}^2}(0)$ we get the width of the rectangle with

$$W = \frac{Q(2 + 4Q^2)}{\omega_0(1 + 4Q^2)} \approx \frac{1}{4 \cdot W_{\text{NE}}} \quad (38)$$

where W_{NE} is defined in (27). By putting the whole area into a Dirac delta function we get the same approximation for $\text{Var}(\xi_2)$ as above

$$\begin{aligned} \text{Var}(\xi_2) &= \frac{I_0^2 \alpha_2^2}{T} \int_{\tau=-T}^T \left(\frac{2C_{y_{\text{noise}}}(0)^2}{4 \cdot W_{\text{NE}}} \right) \delta(\tau) d\tau \\ &= \frac{I_0^2 \alpha_2^2}{T} \left(N_a \cdot W_{\text{NE}} \cdot |H_{\text{mech}}(f_0)|^2 \right)^2 \quad (39) \\ &= \frac{I_0^2 \alpha_2^2}{T} \frac{(N_a \cdot W_{\text{NE}} \cdot |H_{\text{mech}}(f_0)|^2)^2}{2W_{\text{NE}}} \end{aligned}$$

By using our approximations (35) and (36) for $\text{Var}(\xi_1)$ and $\text{Var}(\xi_2)$, respectively, we get an approximation for their ratio

$$\frac{\text{Var}(\xi_1)}{\text{Var}(\xi_2)} \approx \frac{\alpha_1^2 \omega_0^3}{\alpha_2^2 Q^3} \frac{4}{N_a (q/m_{\text{eff}})^2} \quad (40)$$

In the numerical results in Section VI we show the importance of taking the previously neglected term $\text{Var}(\xi_1)$ into account for the accurate analysis of the nanotube receiver.

B. Received Signal Analysis

In the analysis, we consider the steady-state response for the signal component, i.e., we assume that T is large as compared to the transient period. In the steady-state

$$\text{E}\{y_{\text{recv}}(t, \phi)\} = E_{\text{rad}} |H_{\text{mech}}(f_c)| \cos(2\pi f_c t + \phi) \quad (41)$$

where f_c is the frequency of the sinusoidal (transmitted tone), and the phase component ϕ includes the phase shifting by the CNT [20] and a random carrier phase so that ϕ can be modeled as random variable uniformly distributed between 0 and 2π . The H_{mech} is the response of the CNT at frequency f_c which is found with (1). Also,

$$\text{E}\{y_{\text{recv}}(t, \phi)^2\} = \text{E}\{y_{\text{recv}}(t, \phi)\}^2 + C_{y_{\text{noise}}}(0), \quad (42)$$

We assume that the phase is constant for one pulse, but independent and identically distributed over different transmitted pulses. By integrating over the phase ϕ and t , we get the mean with

$$\begin{aligned} \text{E}(\xi_{\text{recv}}) &= \frac{I_0}{2\pi T} \int_{\phi=0}^{2\pi} \int_{t=0}^T (\alpha_2 \text{E}\{y_{\text{recv}}(t, \phi)^2\} \\ &\quad + \alpha_1 \text{E}\{y_{\text{recv}}(t, \phi)\} + 1) dt d\phi \\ &= \text{E}(\xi_{\text{noise}}) + \frac{I_0 E_{\text{rad}}^2 \alpha_2 |H_{\text{mech}}(f_c)|^2}{2}. \quad (43) \end{aligned}$$

which corresponds to the result in [17]. The mean does not depend on the bit interval T due to averaging over ϕ . The variance is $\text{Var}(\xi_{\text{recv}}) = \text{E}(\xi_{\text{recv}}^2) - \text{E}(\xi_{\text{recv}})^2$, where

$$\begin{aligned} \text{E}(\xi_{\text{recv}}^2) &= \frac{1}{2\pi T^2} \\ &\quad \cdot \int_{\phi=0}^{2\pi} \int_{t_1=0}^T \int_{t_2=0}^T \text{E}(g_1(y_{\text{recv}}(t_1, \phi)) \\ &\quad \cdot g_1(y_{\text{recv}}(t_2, \phi))) dt_2 dt_1 d\phi. \quad (44) \end{aligned}$$

Let us denote $x = y_{\text{recv}}(t_1, \phi)$ and $y = y_{\text{recv}}(t_2, \phi)$. Now we expand $\text{E}(g_1(y_{\text{recv}}(t_1, \phi))g_1(y_{\text{recv}}(t_2, \phi)))$ as in the noise-only case and use the well-known results for moments of multivariate normal variables with non-zero mean. For example,

$$\begin{aligned} \text{E}\{x^2 y^2\} &= \mu_x^2 \mu_y^2 + C_{y_{\text{noise}}}(0)^2 + 2C_{y_{\text{noise}}}(t_2 - t_1)^2 \\ &\quad + C_{y_{\text{noise}}}(0) (\mu_x^2 + \mu_y^2) + 4C_{y_{\text{noise}}}(t_2 - t_1) \mu_x \mu_y, \quad (45) \end{aligned}$$

where we have used $t_2 - t_1$ since we integrate over t_2 and t_1 in (44) and for a given phase ϕ

$$\mu_x = E_{\text{rad}} |H_{\text{mech}}(f_c)| \cos(2\pi f_c t_1 + \phi), \quad (46)$$

$$\mu_y = E_{\text{rad}} |H_{\text{mech}}(f_c)| \cos(2\pi f_c t_2 + \phi). \quad (47)$$

Substituting the expansion to (44), integrating, and using $\text{Var}(\xi_{\text{recv}}) = \text{E}(\xi_{\text{recv}}^2) - \text{E}(\xi_{\text{recv}})^2$ we get (70) in Appendix D. Reasonable good approximation is obtained by using only the component of the first part that includes multiplication by T , i.e.,

$$\begin{aligned} \text{Var}(\xi_{\text{recv}}) &\approx \frac{E_{\text{rad}}^2 I_0^2 \alpha_2^2 N_a |H_{\text{mech}}(f_c)|^2 |H_{\text{mech}}(f_0)|^2}{T} \\ &\quad + \text{Var}(\xi_{\text{noise}}). \quad (48) \end{aligned}$$

In the special case of $f_c = f_0$, i.e., the transmitted tone's frequency equals the mechanical resonance frequency of the CNT, this corresponds to the approximation given in [17], where the justifications behind it are presented.

V. MEAN AND VARIANCE WITH EXPONENTIAL CURRENT CONVERSION FUNCTION

In this Section, we derive expressions for the mean and variance of the average-level detector output for both noise and signal with noise cases for the exponential current conversion function (12) in Section II-B2 to obtain theoretical results for the bit error rate for the On-Off keying with the tunneling nanotube receiver [13].

A. Noise Analysis

The mean of the decision statistic for the tunneling nanotube receiver with current conversion function g_2 defined in (12) in noise-only conditions can be found with

$$E(\xi_{\text{noise}}) = \int_{y=-\infty}^{\infty} g_2(y)f(y;\text{OFF})dy, \quad (49)$$

where $f(y;\text{OFF}) = 1/\sqrt{2\pi C_{y_{\text{noise}}}(0)}e^{-\frac{y^2}{2C_{y_{\text{noise}}}(0)}}$ is the PDF of normal distribution with zero-mean and variance $C_{y_{\text{noise}}}(0)$. By performing the integration we get

$$E(\xi_{\text{noise}}) = \frac{c_1}{\sqrt{2C_{y_{\text{noise}}}(0)c_2 + 1}} \quad (50)$$

For getting the variance we need the covariance of $g_2(y_{\text{noise}}(t))$ denoted with $C_{g_2(y_{\text{noise}})}$. As we are dealing here with the exponential function instead of moments for which results are available we have to use joint PDF of the bivariate normal distribution (29) given by

$$f_{XY}(x,y) = \frac{1}{2\pi C_{y_{\text{noise}}}(0)\sqrt{1-\rho^2}} \cdot e^{-\frac{1}{2(1-\rho^2)}\left[\frac{(x-\mu_x)^2+(y-\mu_y)^2-2\rho(x-\mu_x)(y-\mu_y)}{C_{y_{\text{noise}}}(0)}\right]}, \quad (51)$$

where

$$\rho(\tau) = \frac{C_{y_{\text{noise}}}(\tau)}{C_{y_{\text{noise}}}(0)} = \frac{ue^{-|\tau|v} - ve^{-|\tau|u}}{u-v}. \quad (52)$$

Now we get the covariance in noise-only case by setting $\mu_x = 0$ and $\mu_y = 0$ and using

$$\begin{aligned} C_{g_2(y_{\text{noise}})}(\tau) &= E(g_2(x)g_2(y)) - E(\xi_{\text{noise}})^2 \\ &= \int_y \int_x g_2(x)g_2(y)f_{XY}(x,y)dydx - E(\xi_{\text{noise}})^2 \\ &= c_1^2(1+4c_2C_{y_{\text{noise}}}(0)-4c_2^2(-1+\rho(\tau)^2)C_{y_{\text{noise}}}(0)^2)^{-1/2} \\ &\quad - E(\xi_{\text{noise}})^2 \end{aligned} \quad (53)$$

Finally, we get the variance of the average-level detector output as

$$\text{Var}(\xi_{\text{noise}}) = \frac{1}{T} \int_{\tau=-T}^T (1-|\tau|/T)C_{g_2(y_{\text{noise}})}(\tau)d\tau \quad (54)$$

which can be integrated numerically.

B. Received Signal Analysis

For the tunneling nanotube receiver we get the mean with

$$E(\xi_{\text{recv}}) = \frac{1}{2\pi T} \int_{\phi=0}^{2\pi} \int_{t=0}^T \int_{y=-\infty}^{\infty} g_2(y)f(y;\text{ON})dydt d\phi. \quad (55)$$

Above $f(y;\text{ON})$ refers to the PDF of normal distribution with mean $E_{\text{rad}}|H_{\text{mech}}(f_c)|\cos(2\pi f_c t + \phi)$ and variance $C_{y_{\text{noise}}}(0)$. By combining terms inside the exponential we can integrate over y

$$E(\xi_{\text{recv}}) = \frac{1}{2\pi T} \frac{c_1}{\sqrt{2C_{y_{\text{noise}}}(0)c_2 + 1}} \cdot \int_{\phi=0}^{2\pi} \int_{t=0}^T e^{-\frac{c_2(E_{\text{rad}}|H_{\text{mech}}(f_c)|\cos(2\pi f_c t + \phi))^2}{2C_{y_{\text{noise}}}(0)c_2 + 1}} dt d\phi \quad (56)$$

where the integration over ϕ and t can be done numerically. We get variance with

$$\text{Var}(\xi_{\text{recv}}) = E(\xi_{\text{recv}}^2) - E(\xi_{\text{recv}})^2, \quad (57)$$

where $E(\xi_{\text{recv}})$ is given by (56) and

$$E(\xi_{\text{recv}}^2) = \frac{1}{2\pi T^2} \cdot \int_{\phi=0}^{2\pi} \int_{t_1=0}^T \int_{t_2=0}^T E(g_2(y_{\text{recv}}(t_1,\phi))g_2(y_{\text{recv}}(t_2,\phi))) dt_2 dt_1 d\phi. \quad (58)$$

By integrating over the bivariate normal PDF we get

$$\begin{aligned} E(g_2(y_{\text{recv}}(t_1,\phi))g_2(y_{\text{recv}}(t_2,\phi))) &= \left[c_1^2 \exp\left(\frac{c_2(\mu_x^2 + \mu_y^2 + 2c_2(\mu_x^2 + \mu_y^2 - 2\mu_x\mu_y\rho(\tau))C_{y_{\text{noise}}}(0))}{4c_2C_{y_{\text{noise}}}(0)(-1+c_2(-1+\rho(\tau)^2)C_{y_{\text{noise}}}(0))-1}\right) \right] \\ &= \left[\frac{c_1^2 \exp\left(\frac{c_2(\mu_x^2 + \mu_y^2 + 2c_2(\mu_x^2 + \mu_y^2 - 2\mu_x\mu_y\rho(\tau))C_{y_{\text{noise}}}(0))}{4c_2C_{y_{\text{noise}}}(0)(-1+c_2(-1+\rho(\tau)^2)C_{y_{\text{noise}}}(0))-1}\right)}{\sqrt{1+4c_2C_{y_{\text{noise}}}(0)-4c_2^2(-1+\rho(\tau)^2)C_{y_{\text{noise}}}(0)^2}} \right], \end{aligned} \quad (59)$$

where μ_x and μ_y are defined at the end of Section IV and $\tau = t_2 - t_1$.

VI. NUMERICAL RESULTS

In all of the results for the nanotube receiver we use $\alpha_2 = -7.6541 \times 10^{11}$, $\alpha_1 = -2.9014 \times 10^5$, $q = 3 \times 10^{-14}$, based on [16, Table I], and for the tunneling nanotube receiver we use $q = 10^{-15}$, $c_1 = 4.6946 \times 10^{-6}$, $c_2 = 7.5251 \times 10^{17}$, based on [13]. Common to both cases we use $m_{\text{eff}} = 3.7671 \times 10^{-20}$. The utilized values of q are derived assuming capacitance $C = 10^{-16}$ F [16] and from this the charge q at the tip is obtained by multiplying the capacitance with the applied voltage. This results in a much smaller charge q for the tunneling nanotube receiver, since the applied voltage is assumed to be 10 V compared to 300 V for the nanotube receiver.

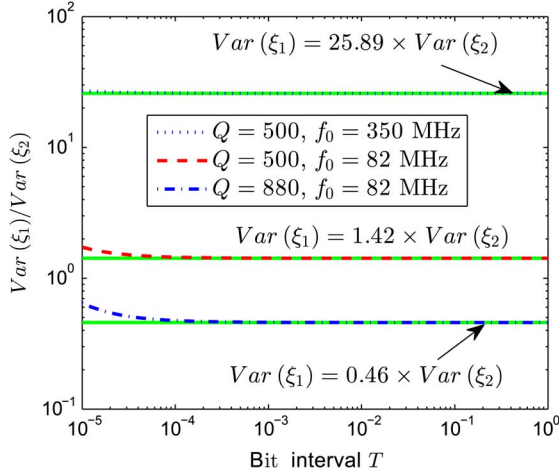


Fig. 5. Ratio of the linear and square-law variance components in digital communication with nanotube receiver as a function of bit interval T . Horizontal solid lines denote results by our approximation (40).

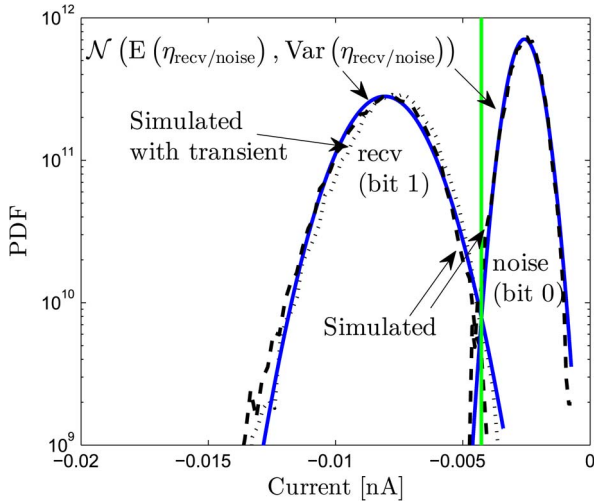


Fig. 6. Simulated and theoretical distribution (normal distribution using the theoretical mean and variance) for $\eta - I_0$ for the nanotube receiver in noise-only (noise) and signal with noise (recv) cases, $Q = 800$, $f_0 = 82$ MHz, $E_{\text{rad}} = 0.547$ V/m, $T = 10^{-4}$ s, $\sigma_{\text{int}}^2 = 0$. Optimal threshold λ^* found with (68) shown as a solid vertical line.

A. Importance of the Linear Component for Variance Calculations

Fig. 5 shows the ratio of the linear (34) and square-law (69) components of the variance in the noise-only case (33). We can see that at some parameters (high frequency, low quality factor) the linear component scaled by α_1 is dominant. Even with higher quality factors and lower frequencies, it has a significant contribution on the total variance and cannot be ignored. Our approximation (40) (horizontal solid lines) is very accurate unless T is small.

B. Gaussian Approximation for the Distribution of the Detector Outputs

1) *Nanotube Receiver*: Fig. 6 shows a comparison between simulated and Gaussian distributions using the theoretical mean and variance values found in Section IV, i.e., the mean found

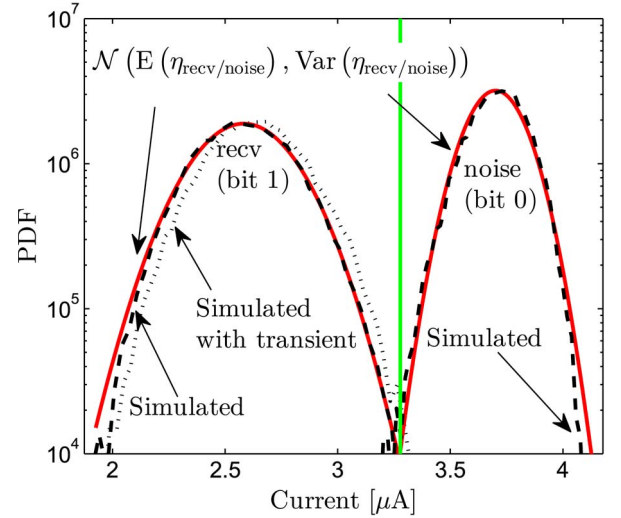


Fig. 7. Simulated and theoretical distribution (normal distribution using the theoretical mean and variance) for η for the tunneling nanotube receiver in noise-only (noise) and signal with noise (recv) cases, $Q = 800$, $f_0 = 82$ MHz, $E_{\text{rad}} = 16.33$ V/m, $T = 10^{-4}$ s, $\sigma_{\text{int}}^2 = 0$. Optimal threshold λ^* found with (68) shown as a solid vertical line.

with (28) (noise-only) and (43) (signal with noise denoted as recv) and variance found with (33) (component values by (34) and (69)) (noise-only) and (70) (signal with noise). To focus on the effects of the receiver type in Fig. 6, we assume no internal noise, i.e., $\sigma_{\text{int}}^2 = 0$.

We show the distribution of $\eta - I_0$ since otherwise the much stronger I_0 is masking the x-axis. For better accuracy in the tails more moments than just mean and variance could be calculated. However, this would be cumbersome and we can already observe very good agreement. Furthermore, we can observe that the transient component does not significantly affect the results. The solid vertical line is the optimal threshold λ^* found with (68).

2) *Tunneling Nanotube Receiver*: Fig. 7 shows comparison between simulated and Gaussian distributions using the theoretical mean and variance values found in Section V, i.e., mean found with (50) (noise-only) and (56) (signal with noise denoted as recv) and variance found with (54) (noise-only) and (57) (signal with noise). To focus on the effects of the receiver type in Fig. 7, we assume no internal noise, i.e., $\sigma_{\text{int}}^2 = 0$ is used in the (21)–(24). A good agreement between theoretical and simulated results can be observed. We can see that when simulations also include the transient part of the output signal there is a small loss in the output. For longer bit intervals T the loss will get smaller and for shorter bit intervals bigger.

C. Bit Error Rates

We used (26) to find the BER with mean and variance values found with the theory in the Section IV (nanotube receiver) and in the Section V (tunneling nanotube receiver) together with (21)–(24) to add the effects of the internal noise to the decision variable.

Fig. 8 present BER as a function of communication distance with 20 dBm transmit power (or 10 dBm transmit power and 10 dB antenna gain), and $T = 10^{-4}$ s. These results have

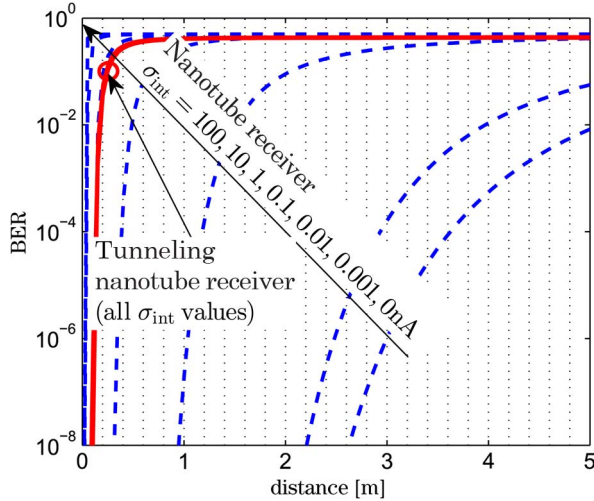


Fig. 8. BER for digital communication for the nanotube and tunneling nanotube receivers, $T = 10^{-4}$ s, $Q = 800$, $f_0 = 82$ MHz, $P_T = 20$ dBm, $V = 300$ (nanotube receiver), $V = 10$ (tunneling nanotube receiver), $q = 3 \times 10^{-14}$ C (nanotube receiver), $q = 10^{-15}$ C (tunneling nanotube receiver), internal noise's standard deviation varied between $\sigma_{\text{int}} = 0\text{--}100$ nA.

been derived by utilizing the optimal threshold λ^* found with (68). Since the transient duration (around 5×10^{-6}) is small compared to T it is not a limiting factor and the maximum bit rate is around 10 000 bits per second provided that BER is sufficiently small. We can see that because of the smaller q the performance of the tunneling nanotube receiver is poor over long distances. Only when distance gets smaller, around 14 cm, the BER reduces to an acceptable level (around 0.001). For longer distances, the nanotube receiver is far superior, even capable of communicating with around 4 meters communication distance. However, the nanotube receiver is very sensitive to internal noise. This is because the distance between mean levels in noise and signal with noise cases is typically very small. For the tunneling nanotube receiver, the distance between the mean levels is much bigger giving it robustness against internal noise. We can read from the figure that when standard deviation of internal noise is 10 nA or more, the performance of the tunneling nanotube receiver is better. When the standard deviation is 1 nA, both receivers give similar performance. When standard deviation is less, the nanotube receiver is better. However, we must keep in mind that the main point in the tunneling nanotube receiver is smaller voltage requirements. Therefore the preferred receiver depends on many factors including targeted communication distance, available voltage, and internal noise level. We also point out that when we increased the internal noise's standard deviation to a very high value of 1 μ A, finally performance of the tunneling nanotube receiver was degrading (not shown in the figure).

Fig. 9 present BER as a function of communication distance with 0 dBm transmit power (or for example -20 dBm transmit power and 20 dB antenna and near-field gain). We can see that even with low transmit power level the tunneling nanotube receiver can be used for around 10 mm distances which is sufficient for communication in nanonetworks [24]. The nanotube receiver leads again to longer or shorter communication distances depending on the internal noise level.

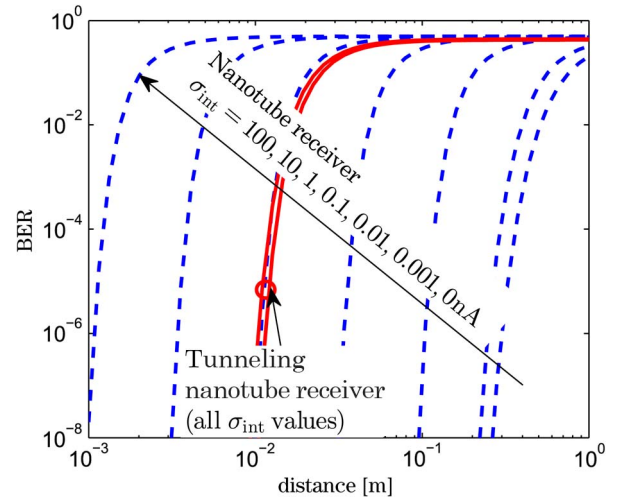


Fig. 9. BER for digital communication for the nanotube and tunneling nanotube receivers, $T = 10^{-4}$ s, $Q = 800$, $f_0 = 82$ MHz, $P_T = 0$ dBm, $V = 300$ (nanotube receiver), $V = 10$ (tunneling nanotube receiver), $q = 3 \times 10^{-14}$ C (nanotube receiver), $q = 10^{-15}$ C (tunneling nanotube receiver), standard deviation varied between $\sigma_{\text{int}} = 0\text{--}100$ nA.

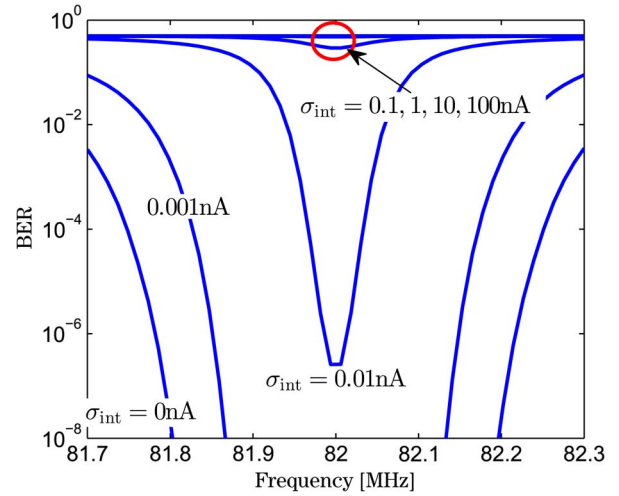


Fig. 10. BER for digital communication for the nanotube receiver as a function of the carrier frequency f_c , $T = 10^{-4}$ s, $Q = 800$, $f_0 = 82$ MHz, $P_T = 20$ dBm, $d = 1$ m, $V = 300$, $q = 3 \times 10^{-14}$ C, $\sigma_{\text{int}} = 0\text{--}100$ nA.

Fig. 10 shows that the best performance is obtained when the transmitted tone frequency f_c is close to the CNT resonance frequency f_0 no matter what is the internal noise level.

VII. THE IMPACT OF THE CNT'S SIZE PARAMETERS

The size parameters (radius and length) have multiple effects. First, they affect the mechanical resonance frequency as described in [7]. The length and radius also affect the amplitude of oscillations due to their effect on the effective mass of the CNT and also on their effect on the charge q at the tip of the CNT. The effective mass is proportional to the product of radius and length. The charge q is also approximately proportional to the product of radius and length [8], [27]. The quality factor depends on the radius and length [28]. Typically, the quality factor increases as length is increased and decreases as radius is increased. As concluded in [28], classical laws cannot fully

explain the dependence of Q on these factors and new theories need to be developed. Higher Q and q reduce the equivalent noise power spectral density N_a . The length and radius also affect the field amplification which can be approximated to be proportional to the ratio between the length and radius of the CNT [27]. Our models are generic and support arbitrary system parameters. However, to get realistic input parameters, we have used parameters based on actual measurements in [16]. The data in [16] are based on CNT which has a length of 1300 nanometers and a radius of 15 nanometers. Due to the limited amount of experimental data available and non-classical behavior, e.g., for Q , it is difficult to give accurate results for other configurations. New physical models and experiments are needed. However, these are out of the scope, as the focus is communication theoretical modeling.

VIII. CONCLUSION

A framework for performance analysis of nanoscale VHF band communication is presented. The objective of this work is to consider both the nanotube (including square-law and linear components) and tunneling nanotube receivers. Theoretical results for the mean and variance for the average-level detector output for noise-only and signal with noise cases are found enabling the calculation of the BER. The results are derived by using the exact correlation function of the CNT tip displacement y with verification by computer simulations. The significance of the analysis stems from the fact that the previously ignored linear component which significantly affects the results is taken into account, and that both exact results and easy to use approximations are presented. Furthermore, the analysis covers the tunneling nanotube receiver for which communication theoretic analysis has not been previously presented. The results confirm that the VHF band is a promising band for nanoscale communication. In future studies, a detailed interference analysis including macro-to-nano interference will be considered. Mixed nanonetworks utilizing both the VHF and the THz bands is also an interesting topic for future research.

APPENDIX A

We find the autocorrelation of $y_{\text{noise}}(t)$ by taking the inverse Fourier transform of its PSD

$$C_{y_{\text{noise}}}(\tau) = \frac{N_a}{2} \left(\frac{q}{m_{\text{eff}}} / (2\pi)^2 \right)^2 \times \int_{f=-\infty}^{\infty} \frac{1}{\left[(f^2 - f_0^2)^2 + \left(\frac{ff_0}{Q} \right)^2 \right]} e^{j2\pi f\tau} df. \quad (60)$$

By following the approach by Slepian in [29] we get

$$C_{y_{\text{noise}}}(\tau) = \varpi \left[\frac{ue^{-|\tau|v} - ve^{-|\tau|u}}{uv(u-v)} \right], \quad (61)$$

where

$$\varpi = \frac{N_a Q}{4\omega_0} (q/m_{\text{eff}})^2 \quad (62)$$

and u and v are complex-valued solutions to

$$uv = \omega_0^2, u^2 + v^2 = \omega_0^2 \left[\frac{1}{Q^2} - 2 \right] \quad (63)$$

satisfying $\text{Re}[u] \geq 0, \text{Re}[v] \geq 0$. In this paper, we utilize the following solution

$$u = \frac{\omega_0}{2Q} - i \frac{\omega_0(\sqrt{4Q^2 - 1})}{2Q}, \quad v = u^* \quad (64)$$

where $(\cdot)^*$ denotes complex conjugate and we have assumed that $Q > 1/2$ which is realistic to enable wireless signal reception. An alternative expression involving only real-values variables

$$C_{y_{\text{noise}}}(\tau) = \frac{\varpi e^{-\frac{\omega_0|\tau|}{2Q}}}{\omega_0^2} \left(\cos \left(\omega_0|\tau| \sqrt{1 - \frac{1}{4Q^2}} \right) + \frac{\sin \left(\omega_0|\tau| \sqrt{1 - \frac{1}{4Q^2}} \right)}{\sqrt{4Q^2 - 1}} \right). \quad (65)$$

The $C_{y_{\text{noise}}}(\tau)$ is also the autocovariance since $y_{\text{noise}}(t)$ is zero-mean. For practical quality factors

$$C_{y_{\text{noise}}}(\tau) \approx \frac{\varpi}{\omega_0^2} e^{-\frac{\omega_0|\tau|}{2Q}} \left(\cos(\omega_0|\tau|) + \frac{\sin(\omega_0|\tau|)}{2Q} \right) \quad (66)$$

and for $Q \gg 1$ we can use

$$C_{y_{\text{noise}}}(\tau) \approx \frac{\varpi}{\omega_0^2} e^{-\frac{\omega_0|\tau|}{2Q}} \cos(\omega_0|\tau|). \quad (67)$$

The above approximation for high values of Q can also be obtained by modeling the response of the filter H_{mech} in (1) as baseband RC-filter upconverted to frequency f_0 and by using the relationship between autocorrelation of bandpass signals and their baseband representation.

APPENDIX B

The critical points for (26) are given in (68), shown at the bottom of the page, where

$$\kappa = \frac{\sqrt{\text{Var}(\eta_{\text{noise}})\text{Var}(\eta_{\text{recv}})}}{\text{Var}(\eta_{\text{noise}}) - \text{Var}(\eta_{\text{recv}})}.$$

$$\lambda^* = \frac{\text{E}(\eta_{\text{recv}})\text{Var}(\eta_{\text{noise}}) - \text{E}(\eta_{\text{noise}})\text{Var}(\eta_{\text{recv}})}{\text{Var}(\eta_{\text{noise}}) - \text{Var}(\eta_{\text{recv}})} \pm \kappa \cdot \sqrt{(\text{E}(\eta_{\text{noise}}) - \text{E}(\eta_{\text{recv}}))^2 + (\text{Var}(\eta_{\text{noise}}) - \text{Var}(\eta_{\text{recv}})) \log \left(\frac{\text{Var}(\eta_{\text{noise}})}{\text{Var}(\eta_{\text{recv}})} \right)} \quad (68)$$

APPENDIX C

$$\begin{aligned} \text{Var}(\xi_2) = & \frac{\bar{\omega}^2}{T^2} \frac{I_0^2 \alpha_2^2}{u^4 v^4 (u+v)^2 (u-v)^2} \\ & \times \left((v^6 e^{-2Tu} - v^6) \right. \\ & + u^6 (e^{-2Tv} + 2Tv - 1) \\ & + u^5 (2ve^{-2Tv} - 2v + 4Tv^2) \\ & + u(2Tv^6 + 2v^5 e^{-2Tu} - 2v^5) \\ & - u^4 (6Tv^3 - v^2 e^{-2Tv} + v^2) \\ & - u^3 (6Tv^4 + 8v^3 e^{-T(u+v)} - 8v^3) \\ & \left. + u^2 (4Tv^5 + v^4 e^{-2Tu} - v^4) \right). \end{aligned} \quad (69)$$

APPENDIX D

$$\begin{aligned} \text{Var}(\xi_{\text{recv}}) = & \frac{4E_{\text{rad}}^2 I_0^2 |H_{\text{mech}}(f_c)|^2 \bar{\omega} \alpha_2^2}{T^2} \\ & \cdot \left(\frac{u\beta^2 - v\alpha^2 + \alpha\beta(u^2 - v^2)T}{\alpha^2 \beta^2 (u-v)} + \frac{4\pi^2 f_c^2 (\alpha^2 u - \beta^2 v)}{\omega_0^2 \alpha^2 \beta^2 (u-v)} \right) \\ & + \frac{E_{\text{rad}}^2 I_0^2 |H_{\text{mech}}(f_c)|^2}{T^2} \\ & \cdot \left(\frac{\alpha_1^2 (1 - \cos(2\pi T f_c))}{4\pi^2 f_c^2} \right. \\ & \left. + \frac{E_{\text{rad}}^2 \alpha_2^2 |H_{\text{mech}}(f_c)|^2}{32\pi^2 f_c^2} (1 - \cos(2\pi T f_c)^2) \right) \\ & + \frac{E_{\text{rad}}^2 I_0^2 |H_{\text{mech}}(f_c)|^2 \bar{\omega} \alpha_2^2}{T^2 \alpha^2 \beta^2 (u-v)} \\ & \cdot (4\cos(2\pi T f_c) (\alpha^2 v e^{-Tv} - \beta^2 u e^{-Tu}) \\ & + 16\pi f_c \sin(2\pi T f_c) (\beta^2 e^{-Tu} - \alpha^2 e^{-Tv}) \\ & + \frac{16}{\omega_0^2} \pi^2 f_c^2 \cos(2\pi T f_c) (\beta^2 v e^{-Tu} - \alpha^2 u e^{-Tv})) \\ & + \text{Var}(\xi_{\text{noise}}). \end{aligned} \quad (70)$$

where $\alpha = (4\pi^2 f_c^2 + u^2)$ and $\beta = (4\pi^2 f_c^2 + v^2)$.

REFERENCES

- [1] I. F. Akyildiz, J. M. Jornet, and M. Pierobon, "Nanonetworks," *Commun. ACM*, vol. 54, no. 11, pp. 84–89, Nov. 2011.
- [2] I. Akyildiz and J. Jornet, "The Internet of nano-things," *IEEE Wireless Commun. Mag.*, pp. 58–63, Dec. 2010.
- [3] I. F. Akyildiz, F. Brunetti, and C. Blázquez, "Nanonetworks: A new communication paradigm," *Comput. Netw.*, vol. 52, no. 12, pp. 2260–2279, Aug. 2008.
- [4] D. Dragoman and M. Dragoman, *Nanomedicine*. Berlin, Germany: Springer-Verlag, Feb. 2012.
- [5] M. Tabesh, M. Rangwala, A. Niknejad, and A. Arbabian, "A power-harvesting pad-less mm-sized 24/60 GHz passive radio with on-chip antennas," in *Proc. Symp. VLSI Circuits Dig. Tech. Papers*, Jun. 2014, pp. 1–2.
- [6] J. Yao *et al.*, "Nanowire nanocomputer as a finite-state machine," *Proc. Nat. Academy Sci.*, vol. 111, no. 7, pp. 2431–2435, 2014.
- [7] K. Jensen, J. Weldon, H. Garcia, and A. Zettl, "Nanotube radio," *Nano Lett.*, vol. 7, no. 11, pp. 3508–3511, Nov. 2007.
- [8] K. J. Jensen, "Nanomechanics of carbon nanotubes," Ph.D. dissertation, Univ. California, Berkeley, CA, USA, 2008.

- [9] I. F. Akyildiz and J. M. Jornet, "Electromagnetic wireless nanosensor networks," *Nano Commun. Netw.*, vol. 1, no. 1, pp. 3–19, Mar. 2010.
- [10] J. Weldon, K. Jensen, and A. Zettl, "Nanomechanical radio transmitter," *Phys. Status Solidi B*, vol. 245, no. 10, pp. 2323–2325, Oct. 2008.
- [11] C. Chen *et al.*, "Graphene mechanical oscillators with tunable frequency," *Nat. Nanotechnol.*, vol. 8, pp. 923–927, 2013.
- [12] C. H. Lee, S. W. Lee, and S. S. Lee, "A nanoradio utilizing the mechanical resonance of a vertically aligned nanopillar array," *Nanoscale*, vol. 6, no. 4, pp. 2087–2093, Feb. 2014.
- [13] D. Dragoman and M. Dragoman, "Tunneling nanotube radio," *J. Appl. Phys.*, vol. 104, no. 7, Oct. 2008.
- [14] V. Gouttenoire *et al.*, "Digital and FM demodulation of a doubly clamped single-walled carbon-nanotube oscillator: Towards a nanotube cell phone," *Small*, vol. 6, no. 9, pp. 1060–1065, May 2010.
- [15] J.-M. Bonard, K. Dean, B. Coll, and C. Klinke, "Field emission of individual carbon nanotubes in the scanning electron microscope," *Phys. Rev. Lett.*, vol. 89, no. 19, pp. 1060–1–1060–5, Oct. 2002.
- [16] P. Vincent *et al.*, "Performance of field-emitting resonating carbon nanotubes as radio-frequency demodulators," *Phys. Rev. B*, vol. 83, no. 15, p. 155446, Apr. 2011.
- [17] C. E. Koksall and E. Ekici, "A nanoradio architecture for interacting nanonetworking tasks," *Nano Commun. Netw.*, vol. 1, no. 1, pp. 63–75, Mar. 2010.
- [18] C. E. Koksall, E. Ekici, and S. Rajan, "Design and analysis of systems based on RF receivers with multiple carbon nanotube antennas," *Nano Commun. Netw.*, vol. 1, no. 3, pp. 160–172, Sep. 2010.
- [19] B. Gulbahar and O. Akan, "A communication theoretical modeling of single-walled carbon nanotube optical nanoreceivers and broadcast power allocation," *IEEE Trans. Nanotechnol.*, vol. 11, no. 2, pp. 395–405, Mar. 2012.
- [20] T. R. Albrecht, P. Grutter, D. Horne, and D. Rugar, "Frequency modulation detection using high-Q cantilevers for enhanced force microscope sensitivity," *J. Appl. Phys.*, vol. 69, no. 2, pp. 668–673, 1991.
- [21] K. L. Ekinci and M. L. Roukes, "Nanoelectromechanical systems," *Rev. Sci. Instrum.*, vol. 76, no. 6, 2005, Art. ID. 061101.
- [22] M. Poot and H. S. van der Zant, "Mechanical systems in the quantum regime," *Phys. Rep.*, vol. 511, no. 5, pp. 273–335, Feb. 2012.
- [23] J. A. Stroscio and R. M. Feenstra, *Scanning Tunneling Microscopy: Volume 27*. San Diego, CA, USA: Academic, 1993.
- [24] J. M. Jornet and I. F. Akyildiz, "Channel modeling and capacity analysis for electromagnetic wireless nanonetworks in the terahertz band," *IEEE Trans. Wireless Commun.*, vol. 10, no. 10, pp. 3211–3221, Oct. 2011.
- [25] S. Miller and D. Childers, *Probability and Random Processes*. New York, NY, USA: Academic, 2004.
- [26] L. Isserlis, "On a formula for the product-moment coefficient of any order of a normal frequency distribution in any number of variables," *Biometrika*, vol. 12, no. 1/2, pp. 134–139, Nov. 1918.
- [27] X. Wang, M. Wang, P. He, Y. Xu, and Z. Li, "Model calculation for the field enhancement factor of carbon nanotube," *J. Appl. Phys.*, vol. 96, no. 11, pp. 6752–6755, 2004.
- [28] A. K. Vallabhaneni, J. F. Rhoads, J. Y. Murthy, and X. Ruan, "Observation of nonclassical scaling laws in the quality factors of cantilevered carbon nanotube resonators," *J. Appl. Phys.*, vol. 110, no. 3, p. 034312, 2011.
- [29] D. Slepian, "Fluctuations of random noise power," *Bell Syst. Tech. J.*, vol. 37, no. 163, pp. 163–184, Jan. 1958.



Janne J. Lehtomäki (S'03–M'06) received his doctorate in wireless communications from the University of Oulu in 2005. Currently, he is a Senior Research Fellow at the University of Oulu, Centre for Wireless Communications. He spent the fall 2013 semester at the Georgia Institute of Technology, Atlanta, USA, as a Visiting Scholar. Currently, he is focusing on communication techniques for networks composed of nanoscale devices. Dr. Lehtomäki has served as a Guest Associate Editor for the *IEICE Transactions on Communications* Special Section

(Feb. 2014) and as a (managing) guest editor for *Nano Communication Networks* Special Issue (Dec. 2015). He co-authored the paper receiving the Best Paper Award in IEEE WCNC 2012. He was TPC Co-Chair for IWSS Workshop at IEEE WCNC 2015 and Publicity Chair for ACM NANOCOM 2015. Dr. Lehtomäki has published more than 100 papers in journals and conference proceedings.



cognitive radio networks, and wireless sensor networks.

A. Ozan Bicen (S'08) received the B.Sc. and M.Sc. degrees in Electrical and Electronics Engineering from Middle East Technical University, Ankara, Turkey, in 2010 and from Koc University, Istanbul, Turkey in 2012, respectively. He is currently a Graduate Research Assistant in the Broadband Wireless Networking Laboratory and pursuing his Ph.D. degree at the School of Electrical and Computer Engineering, Georgia Institute of Technology, Atlanta, GA. His current research interests include design and analysis of molecular communication systems,



of Electrical Engineering at Universitat Politècnica de Catalunya (UPC) in Barcelona, Catalunya, Spain and founded the N3Cat (NaNoNetworking Center in Catalunya). Since September 2012, Dr. Akyildiz is also a FiDiPro Professor (Finland Distinguished Professor Program (FiDiPro) supported by the Academy of Finland) at Tampere University of Technology, Department of Communications Engineering, Finland. He is the Editor-in-Chief of *Computer Networks*, and the founding Editor-in-Chief of the *Ad Hoc Networks*, *Physical Communication*, and *Nano Communication Networks*. He is an IEEE Fellow (1996) and an ACM Fellow (1997). He received numerous awards from IEEE and ACM. His current research interests are in nanonetworks, 5G cellular systems, and wireless sensor networks.

Ian F. Akyildiz (M'86–SM'89–F'96) received the B.S., M.S., and Ph.D. degrees in Computer Engineering from the University of Erlangen-Nurnberg, Germany, in 1978, 1981 and 1984, respectively. Currently, he is the Ken Byers Chair Professor in Telecommunications with the School of Electrical and Computer Engineering, Georgia Institute of Technology, Atlanta, the Director of the Broadband Wireless Networking Laboratory and Chair of the Telecommunication Group at Georgia Tech. Dr. Akyildiz is an honorary professor with the School